Photographic electroluminescence analysis of CIGS thin-film solar modules

Uwe Rau & **Thomas Kirchartz**, IEF5-Photovoltaik, Forschungszentrum Jülich, Germany; **Anke Helbig** & **Jürgen H. Werner**, Institut für Physikalische Elektronik, Universität Stuttgart, Germany; & **Raymund Schäffler**, Würth Elektronik Research GmbH, Schwäbisch Hall, Germany

This paper first appeared in the sixth print edition of *Photovoltaics International* journal.

ABSTRACT

During the past few years, electroluminescence imaging has become a standard characterization technique for failure analysis and qualification of silicon wafer-based solar cells and modules. In contrast, the same analysis is not yet widely used for thin-film modules. This article demonstrates that electroluminescence analysis is a highly suitable tool for the in-depth investigation of Cu(In,Ga)Se_2 thin-film solar modules as well as for standard quality control. The reciprocity between the photovoltaic action and the electroluminescence emission of solar cell devices is used to derive quantitative relations that describe the voltage distribution within a solar module. Individual shunt spots in a module are not only visualized but their influence on the current voltage curves of the individual cells is quantitatively analyzed. Furthermore, device parameters like the sheet resistances of the window layer and the back contact are derived from the electroluminescence images.

Introduction

Less than four years after the pioneering work of Fuyuki et al. [1], photographic electroluminescence (EL) imaging has become an important tool that is almost routinely applied to the characterization of silicon wafer-based solar cells and solar modules [2-9]. Fig 1a depicts the simple experimental setup needed for the EL imaging of a solar cell. Besides a cooled Si-CCD camera, the only requirements are a power supply for the solar cell and an appropriate shielding against parasitic electromagnetic radiation. In some setups, an infrared filter helps to eliminate stray light from the visible part of the spectrum.

> "All important physical processes that influence the photovoltaic performance of a solar cell – like recombination, resistive and optical losses – are complementarily reflected in the EL of the same device."

The attractiveness of EL imaging results on the one hand from its simplicity and swiftness combined with the high spatial resolution that is provided by this technique. An EL image is obtained in less than one second and the technique can be used to survey entire modules but also to visualize microscopic defects on the micrometer scale. On the other hand, EL, i.e. the emission of light by application of an electrical bias, is just the complementary reciprocal action of the photovoltaic effect used in solar cells and modules. Therefore, all important physical processes that influence the photovoltaic performance of a solar cell – like recombination, resistive and optical losses – are complementarily reflected in the EL of the same device, a fact warranting the relevance of the method. In addition to spatially resolved methods, spectrally resolved EL [10-13] has proven to be a suitable tool for the analysis of solar cells. However, the present article concentrates on the photographic, i.e., spatially resolved EL analysis of Cu(In,Ga)Se_2 (CIGS) modules.

Basics

Electroluminescence, or the emission of light in consequence to the application of a forward voltage bias, is the reciprocal action to the standard operation of a solar cell, namely the conversion of incident light into electricity. According to the reciprocity theorem, the EL intensity ϕ_{em} of a pn-junction solar cell emitted at any position $\mathbf{r} = (x,y)$ of the solar cell's surface is given by [14]

$$\phi_{em}(E,\mathbf{r}) = [1-R(\mathbf{r})]Q_i(\mathbf{r})\phi_{bb}(E)\exp\left(\frac{qV(\mathbf{r})}{kT}\right) = Q_e(E,\mathbf{r})\phi_{bb}(E)\exp\left(\frac{qV(\mathbf{r})}{kT}\right) \quad (1)$$

where kT/q is the thermal voltage, $V(\mathbf{r})$ is the internal junction voltage, E is the photon energy, and $Q_e(\mathbf{r}) = [1-R(\mathbf{r})]Q_i(\mathbf{r})$ is the local external quantum efficiency determined by the front surface reflectance $R(\mathbf{r})$ and the internal quantum efficiency $Q_i(\mathbf{r})$. The spectral photon density ϕ_{bb} of a black body

$$\phi_{bb}(E) = \frac{2\pi E^2/(h^3c^2)}{\exp(E/kT)-1} \quad (2)$$

depends on Planck's constant h and the vacuum speed c of light. Recording the EL emission of a solar cell with a charge-coupled device (CCD) camera, the EL signal $S_{cam}(E,\mathbf{r})$ in each camera pixel is

$$S_{cam}(\mathbf{r}) = \int Q_{cam}(E)Q_e(E,\mathbf{r})\phi_{bb}(E)dE\exp\left(\frac{qV(\mathbf{r})}{kT}\right) \quad (3)$$

where Q_{cam} is the energy-dependent sensitivity of the detecting camera. Since in Equation 3 $\phi_{bb}(E)$ and $Q_{cam}(E)$ depend on the energy but not on the surface position $\mathbf{r}$, lateral variations in the detected EL intensity emitted from different surface positions originate only from the lateral variations of the external quantum efficiency Q_e and of the internal voltage V. Hence, Equation 1 and thus Equation 3 consider all losses occurring in solar cells: the external quantum efficiency Q_e expresses the recombination and optical losses, while the internal voltage V reflects the resistive losses. Especially for the surveying of photovoltaic modules, the exponential voltage-dependent term dominates the image, making EL analysis a tool that is especially suitable to analyze resistive losses.

Results and discussion

Electroluminescence analysis of thin-film modules is not yet as common as it is for wafer-based solar cells. Nevertheless, the suitability and the potential of EL analysis of these devices is perfectly analogous to that of silicon cells. The following discusses the investigation of a CIGS module [15,16] as a general example of the analysis of a thin-film module. Variations of the material quality and stoichiometry in CIGS solar cells occur on relatively small length scales between

5µm and 20µm [17,18] and would therefore require microscopic investigations of the luminescence [19-23].

However, prominent features in EL images on the module level are predominantly due to resistive effects, i.e. either caused by series resistances or by shunts as can be seen from Fig. 2 where EL images of a CIGS module are displayed taken at two different current densities J = 1.25mA/cm² (a) and at J = 50mA/cm² (b). The module consists of N_c = 42 cells connected in series with a single cell area of 20 × 0.4cm². The image taken at the lower current (Fig. 2a) shows dark cells at the top of the module (i.e. for low x-values) as the most prominent feature. When increasing the current to J = 50mA/cm² , all cells appear bright over their whole width (i.e. extension in y-direction). However, circular dark spots especially in the upper right corner remain visible. In addition, every cell in Fig. 2b shows a characteristic intensity gradient from high intensity at the top to low intensity at the bottom with only little variation in the y-direction. This intensity gradient is not visible in the image taken with the lower bias current (Fig. 2a).

The macroscopic analysis discussed in the following is an example of where it is reasonable to assume that $Q_e(E,\mathbf{r})$ is almost spatially independent, especially because the exponential dependence of the variations of the internal junction voltage $V(\mathbf{r})$ have a much stronger impact on the EL intensity than possible spatial variations of $Q_e(\mathbf{r})$. Thus, assuming a spatially- and voltage-independent Q_e rearranges Equation 3 to

$$S_{cam}(\mathbf{r}) = \int Q_{cam}(E) Q_e(E) \phi_{bb}(E) dE \exp\left(\frac{qV(\mathbf{r})}{kT}\right) \quad (4)$$

Consequently, we can determine from S_{cam} the voltage drop over the junction (see Equation 5 [right]), except for a spatially constant offset voltage V_{offs}.

Fig. 3 visualizes the application of Equation 5 to the EL data from Fig. 2 to obtain the relative voltage ΔV as a function of the coordinate x across all cells in the module. Note that we have generated the line scan by averaging over the y-coordinate, i.e., over the whole length of the module. Two important features are immediately evident from these line scans: first, the relatively

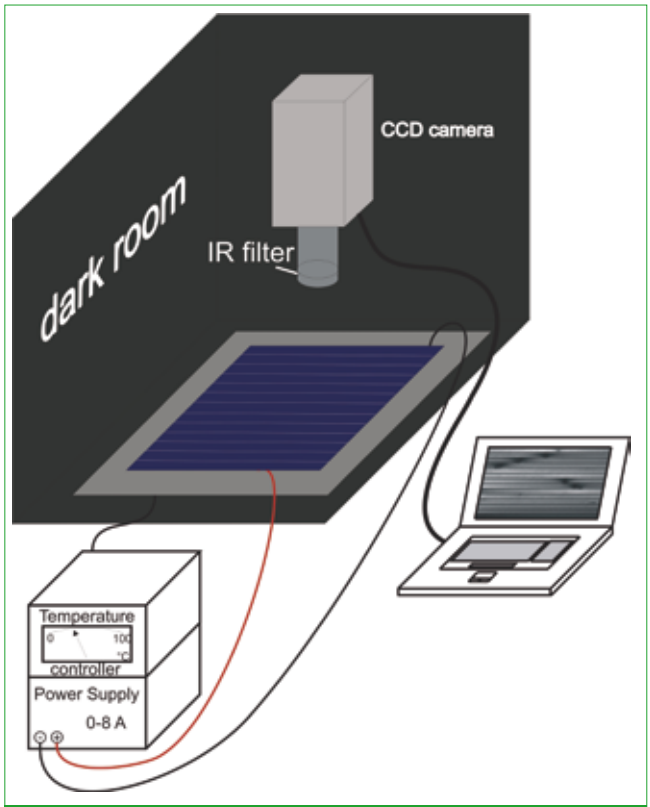

Figure 1. Sketch of the experimental setup for the photographic survey of solar cells or solar modules.

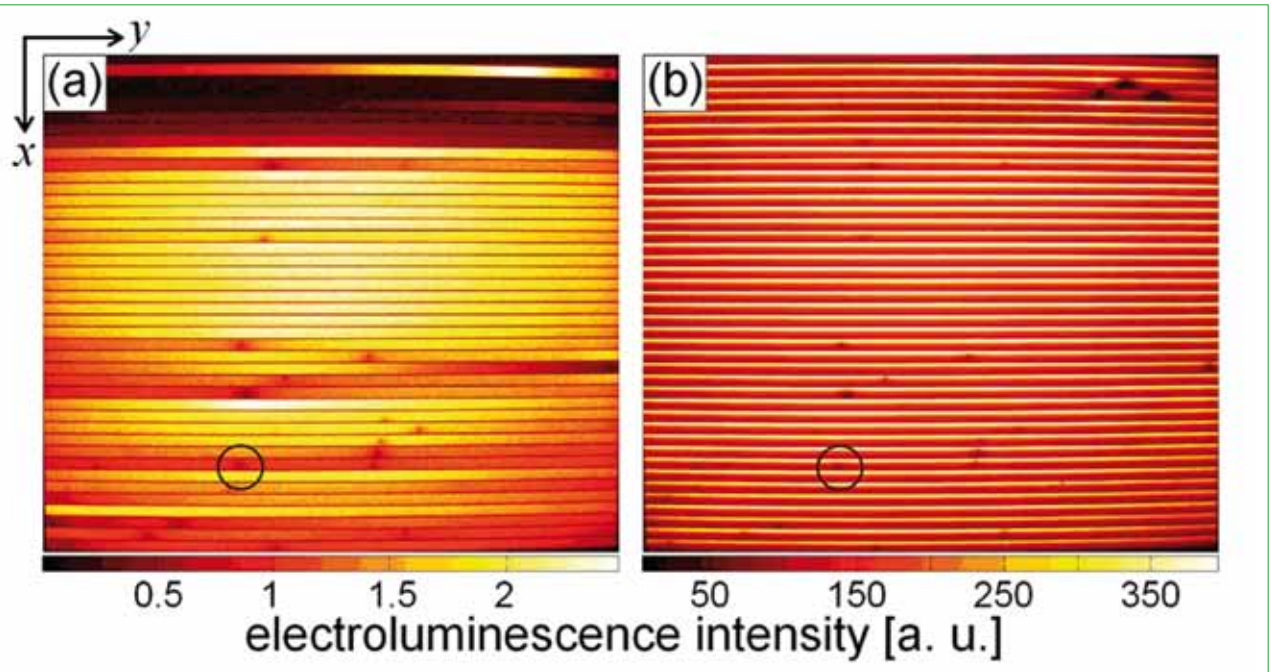

Figure 2. EL images at a) J = 1.25mA/cm² and b) J = 50mA/cm² of the same Cu(In,Ga)Se_2 module. Areas with quenched EL intensity are caused by shunts (see shunt highlighted by circle). Shunts have a larger influence on the current distribution through the cell when current densities are small as in (a), since the pn-junction has a non-linear J/V characteristic. For the same reason, the EL intensity drop in the x direction becomes steeper as the current density increases.

low voltage drop over some cells due to the shunts. This feature is especially visible at low current bias J = 1.25mA/cm² and tends to disappear with increasing bias. Second, there are voltage losses across individual cells due to the sheet resistance of window and back contact layer. This feature becomes increasingly important at larger current bias and is clearly visible for the curves corresponding J = 1.25mA/cm² and 25mA/cm² in Fig. 3.

"Fitting parameters are the sheet resistances ρ^{sq}_{ZnO} of the ZnO and ρ^{sq}_{Mo} of the Mo back contact as well as the differential junction conductance G_D at each bias point."

For a more quantitative access to the data in Fig. 3 we need to model the voltage distribution along the whole width w of one sub-cell. This requires the solution of the coupled current continuity equations in the window layer and in the back contact [16]. In one dimension, we have

$$\frac{d^2}{dx^2}V_1 = -\rho_1^{sq}\frac{d}{dx}j_1^p = \rho_1^{sq}J(V) \qquad (6)$$

and

$$\frac{d^2}{dx^2}V_2 = -\rho_2^{sq}\frac{d}{dx}j_2^p = -\rho_2^{sq}J(V) \qquad (7)$$

where $V_{1,2}$ denote the voltages, $j^p_{1,2}$ are the line current densities, and $\rho^{sq}_{1,2}$ are the sheet resistances of the window layer and the back contact, respectively. The solution of Equations 6 and 7 is given by the voltage difference (see Equation 8 [right]) with the inverse characteristic length $\lambda = [G_D(\rho_1^{sq} + \rho_2^{sq})]^{1/2}$ and $G_D = dJ/dV$ as the differential conductance at the given bias conditions.

For the investigation of the sheet resistances, EL images of a non-shunted region of the module were recorded with a higher spatial resolution. Figure 4 shows the ΔV values calculated from the EL signals across a single non-shunted cell in x direction for three exemplary different bias current densities J = 50, 25, 5mAcm^{-2}. Note that we have averaged the signals over 1376

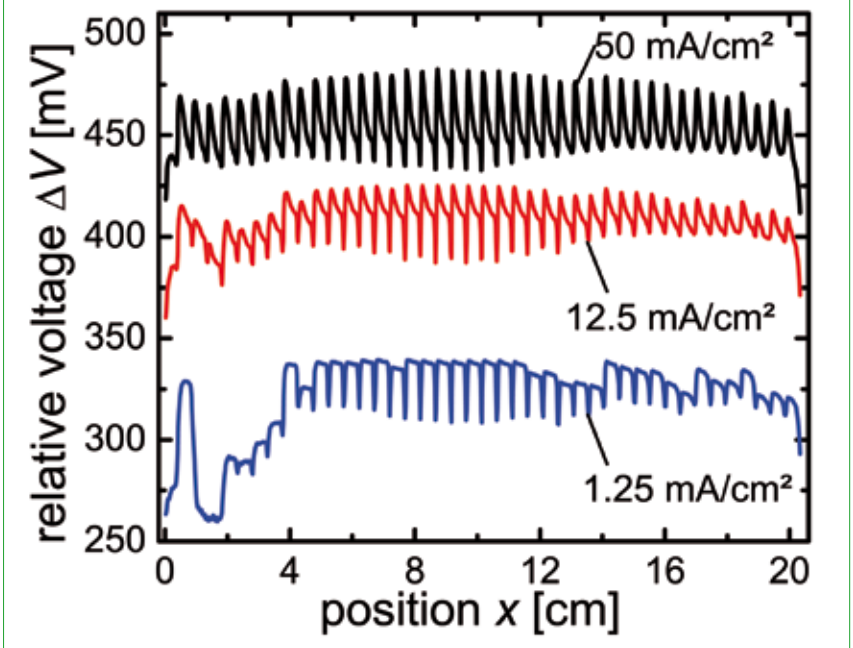

Figure 3. Internal voltage line scans (x-direction) of the whole module of Fig. 2 taken at different bias current densities J_D = 50, 12.5, 1.25mA/cm². The effect of shunts on the voltage is more pronounced for smaller than for higher injection current densities. This effect is most obvious for the cells located at positions 1cm < x < 4cm. The line scans are averaged over the whole module length l.

lines in y-direction (corresponding to a width of 3.8cm).

In order to fit the experimental data, we have the choice either to determine the junction conductance G_D from an additional measurement of J_{SC}/V_{OC} independently (as in [16]) or to include the G_D values at each bias point into the fitting procedure. The latter method is based on the EL experiment alone and has the advantage of not needing an extra calibration measurement. The solid lines in Fig. 3 show the result of a simultaneous fit of Equation 8 to the experimental data obtained for the different bias current densities. Fitting parameters are the sheet resistances ρ^{sq}_{ZnO} of the ZnO and ρ^{sq}_{Mo} of the Mo back contact as well as the differential junction conductance G_D at each bias point. It is interesting to note here that the extraction of the smaller of the two sheet resistances (ρ^{sq}_{Mo} in the present case) is possible as soon as a minimum in the $\Delta V(x)$ curves becomes visible as in the topmost curves of Fig. 3.

The fit to the data in Fig. 3 yields $\rho^{sq}_{ZnO} = 18.2\,\Omega/\mathrm{sq}$ and $\rho^{sq}_{Mo} = 1.1\,\Omega/\mathrm{sq}$. Since these values are very close to the results of the calibrated method ($\rho^{sq}_{ZnO} = 18.0\,\Omega/\mathrm{sq}$, $\rho^{sq}_{Mo} = 1.3\,\Omega/\mathrm{sq}$)[16], we conclude that the determination of the sheet resistances from the EL data alone, i.e. without additional calibration measurement, is reasonably reliable. Furthermore, the extraction of both sheet resistance values – that of the window and that of the back contact layer – are possible simultaneously, although the values differ by more than one order of magnitude.

The data in Fig. 2 allow us not only to analyze the voltage drop over individual cells in order to determine the sheet resistance of the window and the back contact layer. We may also compare the voltages that drop over different cells in order to evaluate the relative performance of those cells. These voltage differences are basically caused by the shunts on the various cell stripes of the module, seen as black spots in Fig. 2. As a valid representation of the cell voltage, we take the spatial average of the relative voltages ΔV determined across the cell. Again, we have the option to calibrate the measurement with an additional J_{SC}/V_{OC} measurement which allows us to deduce absolutely scaled J/V curves of all individual cells [16]. In practice, one might wish to avoid such additional measurements. In this case, only voltages shifted by an unknown offset are feasible because of the unknown offset voltage given in Equation 5.

However, determining the scatter of the individual cell voltages at different bias conditions is quite attractive for inline control during the production of thin-film modules. This possibility for a simple EL imaging-based quality control method is illustrated by the histograms in Fig. 5 for three different bias current densities. For these histograms, the cell voltages V_i^{meas} (for the cells $i = 1 \,..\, N_{cell}$) are calculated from the measured EL signal converted via Equation 5 into $\Delta V\,(x,y)$ values and finally averaged over the entire cell area. As expected from our observations in Fig. 2, the influence of shunts on the voltage distribution is highest at low bias currents leading accordingly to a wide distribution of cell voltages. At higher bias currents the discrepancy between the voltages of shunted and non-shunted cells becomes smaller and the distribution becomes narrower. Such histograms as shown in Fig. 5 might provide a simple tool to judge

$$V(\mathbf{r}) = \frac{kT}{q}\left[\ln\{S_{cam}(\mathbf{r})\} - \ln\left\{\int Q_{cam}(E)Q_e(E)\phi_{bb}(E)dE\right\}\right] = \Delta V(\mathbf{r}) + V_{offs}$$

Equation 5.

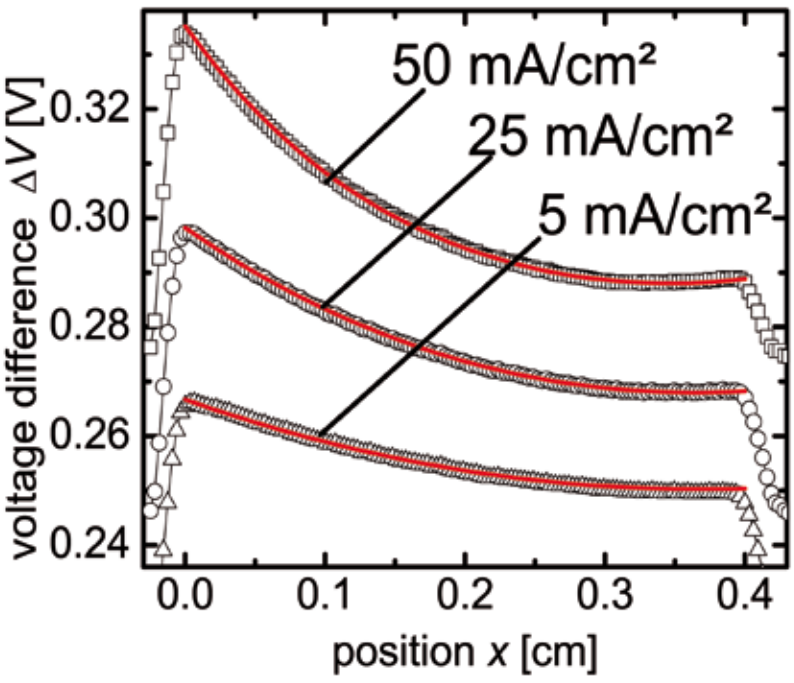

Figure 4. Line scans of the relative internal voltages ΔV calculated from EL line scans. The solid lines represent fits of Equation 8 to the experimental voltage data (open symbols). The sheet resistances used in all fits are ρ^{sq}_{ZnO} = 18Ω/sq and ρ^{sq}_{Mo} = 1.5Ω/sq for the ZnO window layer and for the Mo back contact, respectively. Note that the experimental data are averages over 1376 lines in *y*-direction (corresponding to a width of 3.8cm).

immediately the quality of the module, making EL imaging a suitable tool for inline control containing quantitative information.

> "Determining the scatter of the individual cell voltages at different bias conditions is quite attractive for inline control during the production of thin-film modules."

Finally, we demonstrate the possibility of reconstructing current voltage curves of the individual cells on an absolute scale. Hereto, we consider a series of images taken at different bias current densities and determine the cell voltages V_i^{meas} as described above. Since V_i^{meas} differs from the real cell voltage V_i by an unknown but constant offset voltage V_{offs}, we need to scale the experimental data by one additional measurement. For this purpose, we measure the open circuit voltage V_{OC} of the solar module under illumination. The illumination intensity is adjusted in such a way that the corresponding short circuit current density J_{SC} equals one of the bias current

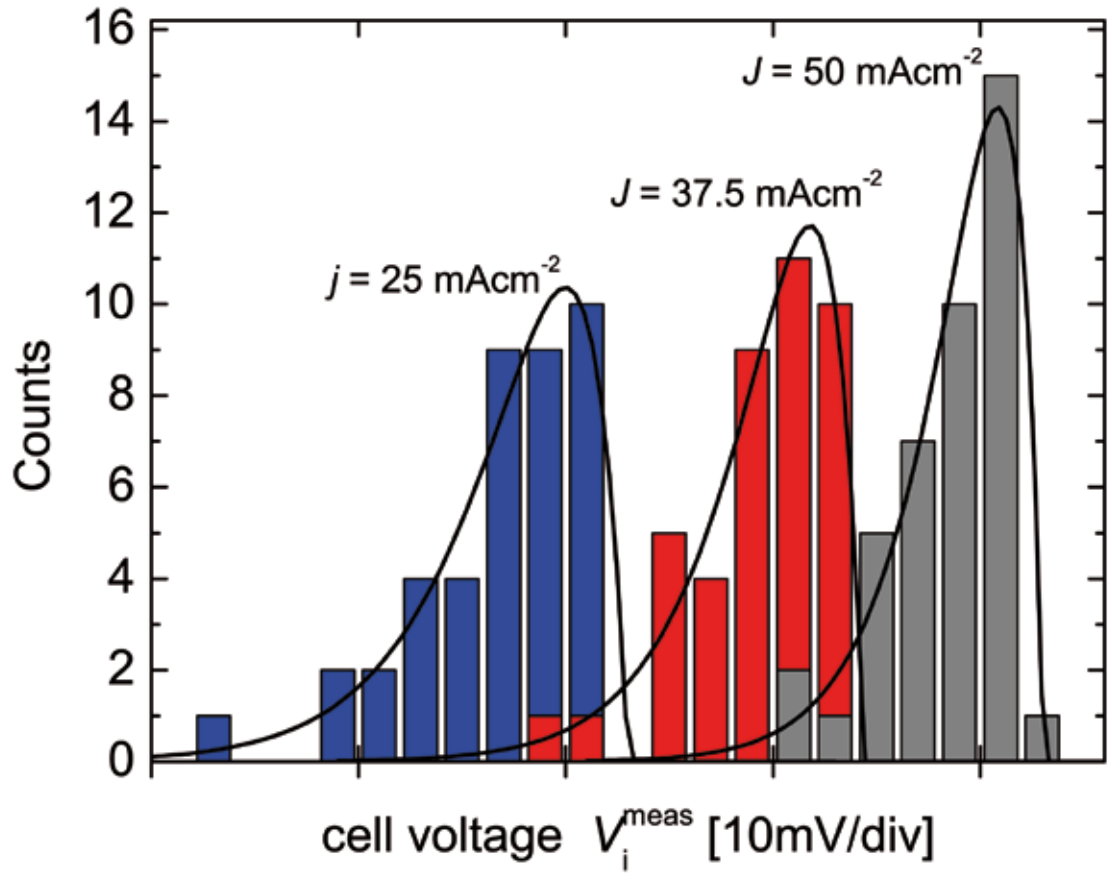

Figure 5. Histogram of the relative cell voltage V_i^{meas} over the cells of the module in Fig. 2. Note that the measured voltages V_i^{meas} differ from the real cell voltage by an unknown but constant offset voltage V_{offs}. The black lines are a guide, illustrating that the voltage distributions become narrower with increasing current bias *J*.

$$\Delta V = -\frac{j^{p}_{max}\rho_{1}^{sq}}{\lambda}\sinh(\lambda x) + \frac{j^{p}_{max}\left[\rho_{1}^{sq}\cosh(\lambda w) + \rho_{2}^{sq}\right]}{\lambda \sinh(\lambda w)}\cosh(\lambda x) + const$$

Equation 8.

densities J used for the EL images. The hitherto unknown offset voltage V_{offs} is then calculated from the equation

$$V_{OC} = \sum_{i=1}^{N_{cell}} V_i = \sum_{i=1}^{N_{cell}} V_i^{meas} - N_{cell}V_{offs} \quad . \qquad (9)$$

It is important to acknowledge that taking the open circuit voltage V_{OC} as a reference is more suitable for a proper scaling than using the voltage V_{mod} that is applied to the module during the actual measurement. This is because V_{mod} not only contains the sum of the cell voltages V_i but also the voltage losses due to the series resistance R_S within the module that we have at a given bias current J instead of Equation 9

$$V_{mod} = \sum_{i=1}^{N_{cell}} V_i + JR_S = \sum_{i=1}^{N_{cell}} V_i^{meas} - N_{cell}V_{offs} + JR_S \qquad (10)$$

The sum on the right-hand side of Equation 10 contains as an additional unknown quantity the series resistance R_s, that might even be different for each bias current J. The determination of V_{offs} from V_{mod} is therefore not easy and we use the J_{SC}/V_{OC} method with only one unknown quantity for all bias points, namely V_{offs}.

> "Photographic EL imaging is a promising tool for routine inline inspection of CIGS thin-film modules as well as for in-depth failure analysis."

Fig. 6 displays the scaled current voltage curves J/V_i (open circles) of all cells obtained from a series of EL measurements at different bias currents J. Additionally shown is the $J/\Sigma V_i$ (open diamonds) curve obtained from summing up the internal voltages V_i and, for comparison, the J_{SC}/V_{OC} curve of the module (filled stars), which was used to scale the offset voltage according to Equation 9. As expected from our observations in Figs. 2 and 5, the voltages of the individual cells show a large scatter at low currents whereas at higher currents the discrepancy between the voltages of shunted and non-shunted cells becomes smaller and the data points increasingly coincide. We have thus demonstrated how to assess all individual current voltage curves of a thin-film module by analyzing EL images combined with a simple calibration process.

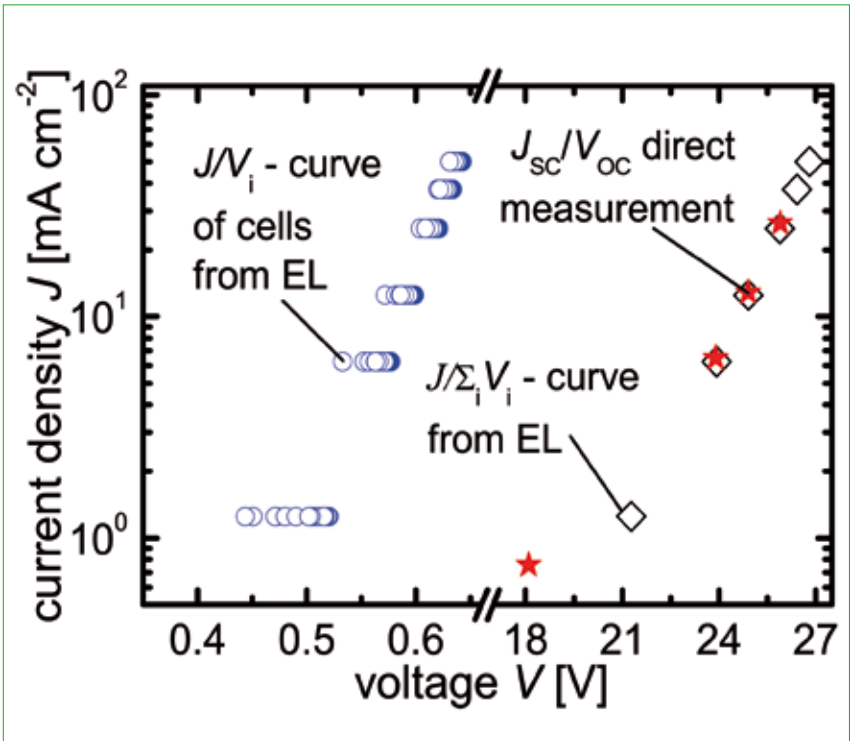

Figure 6. Current density/voltage (J/V_i) curves (open circles) of individual subcells of the module in Fig. 2 determined from their EL emission. For any given J, the corresponding relative individual voltages V_i are taken from line scans of the voltage difference ΔV as shown in Fig. 3. To correct the data for the unknown offset voltage, the sum ΣV_i (diamonds) of the internal voltages V_i of all subcells is adjusted to the J_{SC}/V_{OC} curve of the complete module (stars).

Summary and outlook

Photographic EL imaging is a promising tool for routine inline inspection of CIGS thin-film modules as well as for in-depth failure analysis. In this paper, we have demonstrated how to determine the sheet resistance of the ZnO window layer and of the Mo back contact directly from EL data. Further, we have shown that the voltages across all individual cells within a module at any bias current are measurable by EL imaging except for an unknown offset voltage. Thus, the relative performance of the cells can be judged immediately from an EL image. Scaling such results for various applied currents with a single additional measurement of the open circuit voltage enables us to determine the absolute current/voltage curve of each individual cell in the module. Thus, valuable and detailed information is gained in a straightforward way from easily and swiftly feasible measurements. We note that the present results are only a first step in employing the wealth of information contained in the EL images of CIGS thin-film solar modules. Furthermore, the methods outlined in this paper should be applicable to other types of thin-film modules as well.

References

[1] Fuyuki, T., Kondo, H., Yamazaki, T., Takahashi, Y. & Uraoka, Y. 2005, "Photographic surveying of minority carrier diffusion length in polycrystalline silicon solar cells by electroluminescence", *Appl. Phys. Lett.* Vol. 86, 262108.

[2] Ramspeck, K., Bothe, K., Hinken, D., Fischer, B., Schmidt, J. & Brendel, R. 2007, "Recombination current and series resistance imaging of solar cells by combined luminescence and lock-in thermography", *Appl. Phys. Lett.* Vol. 90, 153502.

[3] Kasemann, M., Schubert, M.C., The, M., Köber, M., Hermle, M. & Warta, W. 2006, "Comparison of luminescence imaging and illuminated lock-in thermography on silicon solar cells", *Appl. Phys. Lett.* Vol. 89, 224102.

[4] Würfel, P., Trupke, T., Puzzer, T., Schäffer, E., Warta, W. & Glunz, S.W. 2007, "Diffusion lengths of silicon solar cells from luminescence images", *J. Appl. Phys.* Vol. 101, 123110.

[5] Breitenstein, O., Bauer, J., Trupke, T. & Bardos, R.A. 2008, "On The Detection of Shunts in Silicon Solar Cells by Photo- and Electroluminescence Imaging", *Prog. Photovolt: Res. Appl.*, Vol. 16, p. 325.

[6] Hinken, D., Ramspeck, K., Bothe, K., Fischer, B. & Brendel, R. 2007, "Series resistance imaging of solar cells by voltage dependent electroluminescence", *Appl. Phys. Lett.*, Vol. 91, 182104.

[7] Bothe, K., Ramspeck, K., Hinken, D. & Brendel, R. 2008, "Imaging Techniques for the Analysis of Silicon Wafers and Solar Cells", *ECS Trans.* Vol. 16, p. 63.

[8] Kasemann, M., Grote, D., Walter, B., Kwapil, W., Trupke, T., Augarten, Y., Bardos, R.A., Pink, E., Abbott, M.D. & Warta, W. 2008, "Luminescence Imaging for the Detection of Shunts on Silicon Solar Cells", *Prog. Photovolt.: Res. Appl.*, Vol. 16, p. 297.

[9] Fuyuki, T. & Kitiyanan, A. 2009, "Photographic diagnosis of crystalline silicon solar cells utilizing electroluminescence", *Appl. Phys. A*, Vol. 96, p. 189.

[10] Kirchartz, T., Rau, U., Kurth, M., Mattheis, J. & Werner, J.H. 2007, "Comparative study of electroluminescence from Cu(In,Ga)Se_2 and Si solar cells", *Thin Solid Films*, Vol. 515, 6238.

[11] Kirchartz, T. & Rau, U. 2007, "Electroluminescence analysis of high efficiency Cu(In,Ga)Se_2 solar cells", *J. Appl. Phys.* Vol. 102, 104510.

[12] Kirchartz, T., Rau, U., Hermle, M., Bett, A.W., Helbig, A. & Werner, J.H. 2008, "Internal voltages in GaInP/GaInAs/Ge multijunction solar cells determined by electroluminescence measurements", *Appl. Phys. Lett.*, Vol. 92, 123502.

[13] Kirchartz, T., Helbig, A., Reetz, W., Reuter, M., Werner, J.H. & Rau, U. 2009, "Reciprocity between electroluminescence and quantum efficiency used for the characterization of silicon solar cells", *Prog. Photovolt: Res. Appl.*, Vol. 17, p. 394.

[14] Rau, U. 2007, "Reciprocity relation between photovoltaic quantum efficiency and electroluminescent emission of solar cells", *Phys. Rev. B*, Vol. 76, 085303.

[15] Rau, U., Kirchartz, T., Helbig, A. & Pieters, B.E. 2009, "Electroluminescence imaging of Cu(In,Ga)Se_2 thin film modules", *Mater. Res. Soc. Symp. Proc.* **1165**, M03-04.

[16] Helbig, A., Kirchartz, T., Schäffler, R., Werner, J.H. & Rau, U. (submitted), "Quantitative electroluminescence analysis of resistive losses in Cu(In,Ga)Se_2 thin-film modules", *Sol. Ener. Mat. Sol. Cells.*

[17] Grabitz, P.O., Rau, U., Wille, B., Bilger, G. & Werner, J.H. 2006, "Spatial inhomogeneities in Cu(In,Ga)Se_2 solar cells analyzed by an electron beam induced voltage technique", *J. Appl. Phys.*, Vol. 100, 124501.

[18] Bauer, G.H., Gütay, L. & Kniese, R. 2005, "Structural properties and quality of the photoexcited state in Cu($In_{1-x}Ga_x$)Se_2 solar cell absorbers with lateral submicron resolution", *Thin Solid Films*, Vol. 480, p. 259.

[19] Romero, M.J., Jiang, C.-S., Noufi, R. & Al-Jassim, M.M. 2005, "Photon emission in $CuInSe_2$ thin films observed by scanning tunneling microscopy", *Appl. Phys. Lett.*, Vol. 86, 143115.

[20] Romero, M.J., Jiang, C.-S., Abushama, J., Moutinho, H.R., Al-Jassim, M.M. & Noufi, R. 2006, "Electroluminescence mapping of $CuGaSe_2$ solar cells by atomic force microscopy", *Appl. Phys. Lett.* Vol. 89, 143120.

[21] Gütay, L. & Bauer, G.H. 2005, "Lateral variations of optoelectronic quality of Cu($In_{1-x}Ga_x$)Se_2 in the submicron-scale", *Thin Solid Films*, Vol. 487, p. 8.

[22] Gütay, L. & Bauer, G.H. 2007, "Spectrally resolved photoluminescence studies on Cu(In,Ga)Se_2 solar cells with lateral submicron resolution", *Thin Solid Films*, Vol. 515, 6212.

[23] Bothe, K., Bauer, G.H. & Unold, T. 2002, "Spatially resolved photoluminescence measurements on Cu(In,Ga)Se_2 thin films", *Thin Solid Films*, Vol. 403, p. 453.

About the Authors

Prof. Dr. Uwe Rau obtained his Ph.D. degree in physics from the University of Tübingen in 1991, and subsequently worked as a postdoc at the Max Planck Institute for Solid State Research, Stuttgart, at the Sony Research Center, Yokohama, and at the University of Bayreuth. From 1997 to 2007 he was scientific group leader at the Institute of Physical Electronics, University of Stuttgart. In 2007 he became a full professor at the RWTH Aachen as well as director of the Institute of Energy Research – Photovoltaics (IEF-5) at Research Centre Jülich.

Dr.-Ing. Thomas Kirchartz studied electrical engineering and information technology in Stuttgart and graduated in 2006. Since 2004, he has been doing research on characterization and modelling of different types of solar cells in the group of Uwe Rau in Stuttgart and later in Jülich. He finished his doctoral thesis in 2008 since which time he has been a post-doctoral researcher in Jülich.

Dipl.-Nat. Anke Helbig studied applied natural science at TU Bergakademie Freiberg and received her diploma in 2006. She then worked in the photovoltaics group of Prof. Dr. Hans Joachim Möller in Freiberg. Since 2007 she has been a Ph.D. student at the Institute of Physical Electronics, University of Stuttgart, working on solar cell characterization.

Prof. Dr. Jürgen H. Werner received his Ph.D. degree in physics from the University of Stuttgart in 1983. After working as a scientist at the Max Planck Institute Stuttgart, he was a guest scientist at the IBM T. J. Watson Research Center, in New York and at AT&T Bell Laboratories, New Jersey. In 1991, he moved to the University of Munich. Since 1996 he has been director of the Institute for Physical Electronics, University of Stuttgart, researching and teaching in the field of photovoltaics, micro- and optoelectronics.

Dipl.-Ing. Raymund Schäffler received his degree of electrical engineer (physical electronics) from the University of Stuttgart. He worked as a scientific assistant at the Institute of Physical Electronics (University of Stuttgart) from 1988 to 1996 and at Zentrum für Sonnenenergie und Wasserstoffforschung (ZSW) from 1996 to 1999. Since 1999 he has been working at Würth Solar in such fields/roles as product manager, technology and R&D.

Enquiries

Prof. Dr. Uwe Rau
Institut für Energieforschung-5
(Photovoltaik)
Forschungszentrum Jülich
52425 Jülich
Germany

Tel: 49 (0) 2461 611 554
Fax: 49 (0) 2461 613 735
Email: u.rau@fz-juelich.de
Web: www.fz-juelich.de/ief/ief-5/